

Article

An Increase in the Energy Efficiency of Abrasive Jet Equipment Based on the Rational Choice of Nozzle Geometry

Vadym Baha ¹, Jana Mižáková ²  and Ivan Pavlenko ^{1,2,*} 

¹ Faculty of Technical Systems and Energy Efficient Technologies, Sumy State University, 2, Rymskogo-Korsakova St., 40007 Sumy, Ukraine; v.baga@kttf.sumdu.edu.ua

² Faculty of Manufacturing Technologies with a Seat in Prešov, Technical University of Košice, 080 01 Prešov, Slovakia; jana.mizakova@tuke.sk

* Correspondence: i.pavlenko@cm.sumdu.edu.ua

Abstract: Permanently increasing requirements for the accuracy of abrasive jet machining (AJM) predetermine a need to increase requirements for the rational choice of the related energy-efficient technological equipment. Due to the relatively cheap and high-quality cleaning of materials from contaminants using AJM, the problem of increasing the energy efficiency of the corresponding equipment based on the rational choice of nozzle geometry becomes more topical. This is also because the working nozzle is a consumable part that requires periodic replacements. Therefore, this article deals with rational designing working nozzles as a reliable way to decrease the power consumption of the compressor equipment while engaging in AJM. For this purpose, experimental and numerical studies of the operating processes in the nozzle were carried out. The main idea of increasing the nozzle's efficiency was to reduce the contact area between the working flow and the nozzle. Due to this, the friction of the abrasive material with its walls was decreased. As a result, the AJM was accelerated, and the energy consumption of the corresponding compressor equipment was reduced. The research showed that a decrease in the nozzle's length up to 4 mm increased the flow ratio by 84% and decreased the energy consumption of the 40 kW compressor unit by 4.5 times.

Keywords: ejector; rational geometry; energy efficiency; durability; process innovation



Citation: Baha, V.; Mižáková, J.; Pavlenko, I. An Increase in the Energy Efficiency of Abrasive Jet Equipment Based on the Rational Choice of Nozzle Geometry. *Energies* **2023**, *16*, 6196. <https://doi.org/10.3390/en16176196>

Academic Editor: Satoru Okamoto

Received: 31 July 2023

Revised: 22 August 2023

Accepted: 24 August 2023

Published: 25 August 2023



Copyright: © 2023 by the authors. Licensee MDPI, Basel, Switzerland. This article is an open access article distributed under the terms and conditions of the Creative Commons Attribution (CC BY) license (<https://creativecommons.org/licenses/by/4.0/>).

1. Introduction

An increase in the energy efficiency of technological equipment is one of the critical points according to Industry 4.0 [1] because of the contribution to improving energy efficiency by an average of 15–25% within this strategy implementation [2] while also ensuring the efficiency of enterprises can be realized by rational selection of the manufacturing process [3].

Abrasive jet machining (AJM) is widely used for cleaning the surfaces of various materials [4]. Recently, the trend of using sandblasting cameras has been increasing [5]. This has been facilitated by new types of abrasives, the improvement of sandblasting devices, and the spread of chemical coatings before the application of which the treated surface should be effectively cleaned. AJM allows for cleaning metal surfaces without damaging the surface structure [6]. The appearance of new materials also leads to expanding the possibilities of AJM.

Since the related devices should offer a cost-effective and energy-efficient solution to maintain and enhance equipment performance in the energy industry, ensuring sustainable and environmentally friendly energy production, the problem of developing rational ways to increase their energy efficiency is topical.

Before formulating the primary purpose of the research, the state of the art should be highlighted. Particularly, Ahmed and Chen [7] used the capture factor as a key parameter to describe the performance of the ejector. This coefficient was determined as the mass of the trapped working flow divided by the mass flow rate of the driving flow.

Van den Berghe et al. [8] developed a new 1D transient model for ejectors based on a pipeline analogy for gas-dynamic calculations. This model was based on the non-stationary Euler's equation. Yan et al. [9] checked CFD simulations for the model with two phases within the permissible range of discrepancies. As a result, a positive effect of up to 30% was reached due to the optimization of the nozzle's geometric parameters. This confirmed the significant impact of the nozzle's geometry on its flow characteristics.

Xu et al. [10] studied a phenomenon similar to the abrasive jet nozzle's wear during operation. As a result, it was established that particle size, mass flow rate, and installation position essentially impact the nozzle's wear. Li et al. [11] carried out numerical simulations of the internal flow structure in the jet system. The nozzle diameter was a key parameter affecting the performance and structure of the internal flow. Aronson et al. [12] presented the impact of geometric characteristics on multistage jet ejectors.

Bañon et al. [13] considered the effect of shot blasting for removing significant contaminants. It was determined that increased pressure creates a greater ability for particle erosion. Kwon and Lee [14] also studied AJM. As a result, it was established that particle type, nozzle diameter, pressure, distance, and processing time affect the surface characteristics. Sychuk et al. [15] assessed the following durability of nozzles from various materials: ceramic—1–2 h, cast iron—6–8 h, tungsten carbide—approximately 300 h, and boron carbide—750–1000 h.

The nozzle flow profile also directly affects the velocity distribution of pressure, density, and temperature. It is closely related to the internal losses of the nozzle. Therefore, the performance improvement due to the optimal flow profile is significant. Under similar conditions, the particle capture ratio increases by 8–19% compared to a conventional ejector [16]. Also, Venturi nozzles achieve 4–7 times more aeration performance than circular ones [17].

During the AJM operation, properly mixing the abrasive material with air is also essential. Xi et al. [18] showed the correctness of using high-frequency oscillations to increase the efficiency of mixing two-phase flows. As a result, a significant increase in productivity (up to 14%) was achieved. Also, Han et al. [19] found that sand grains in the nozzle contribute to cavitation flow development. In this case, the concentration range became smaller with an increase in the average diameter. Other achievements in using hydrodynamic cavitation for the enhancement of the efficiency of fluid working medium preparation technologies were discussed by Fesenko et al. [20].

Zabolotnyi et al. [21,22] proposed a technology to obtain long-length, permeable powder materials with uniform density distribution and stable operational characteristics. Somov et al. [23] developed an experimental stand to process powder materials using a vibratory actuator.

Moreover, Sychuk et al. [24] applied a technology of effective abrasive jet machining of parts surfaces. The developed nozzle design allowed for forming an air layer on the inner surface to reduce the contact of the abrasive airflow with the nozzle surface and increase the durability and energy efficiency of the AJM. Finally, Povstyanoy et al. [25] tested the porous nozzle for AJM. As a result, this made it possible to increase the efficiency of material processing significantly.

Thus, AJM needs an energy-intensive unit that consumes energy significantly in a range of 10–100 kW, depending on the application. Using worn nozzles also leads to excessive use of compressed air and abrasive material. The decisive factors for successfully operating the abrasive jet unit are a powerful source of compressed air and an energy-efficient abrasive jet nozzle. This affects the consumption of compressed air and abrasive material and the efficiency of AJM.

Notably, the main factors of AJM are flow rate, an angle between the jet and the machined surface, abrasive fraction and grain size, abrasive concentration in the flow, and the kinetic and dynamic characteristics of the abrasive jet equipment.

Despite many efforts devoted to studying the designs of abrasive jet devices, the following research gaps remain unsolved. Firstly, the determination of the correct values of

flow rate for cylindrical nozzles operating on an abrasive–air mixture is needed. Such a ratio should consider peculiarities of the flow of the working mixture through the nozzle and allow for more precisely evaluating the mass flow rate of the abrasive flow.

Secondly, analytical dependencies for the mass flow rate and the corresponding flow ratio depending on the nozzle’s diameter should be identified. Such dependencies should correspond to the experimentally obtained data and properly approximate them.

Finally, the possibility of a rational choice of geometric characteristics for working nozzles operating on an abrasive–air mixture should be realized.

All the above-mentioned factors should allow for increasing the efficiency of the working nozzles during AJM due to the impact on geometric parameters and operating modes. Therefore, the assumption that the rational choice of the geometrical characteristics can increase AJM efficiency is the central hypothesis of the research.

Overall, the article aims at ensuring the energy efficiency of AJM. The following research objectives were formulated to achieve this goal. Firstly, numerical and experimental studies of AJM for various working nozzles’ geometric parameters and operating modes should be conducted. For this purpose, the experimental stand should be designed.

Secondly, the obtained experimental results should be analyzed in terms of the possibility of ensuring energy efficiency. For this purpose, the regression analysis should be applied. Finally, rational geometric parameters to increase the efficiency of AJM should be developed.

2. Materials and Methods

2.1. Analytical Approach

The approaches to calculating and designing nozzle elements with relatively small cross-sections (e.g., cylindrical and conical nozzles, holes with sharp edges) were based on generalized experimental data. For example, for the labyrinth seal case study, the design was represented as a series of sequentially installed holes with sharp edges. A conditional flow ratio was also introduced. It allowed for considering all the available assumptions and simplifications.

The flow characteristics of the nozzle for AJM were also calculated according to the same principle. However, existing methods of analytical calculation of mass flow through a channel with a sharp edge have differences of up to 30% [26].

Under such circumstances, the fundamental Stodola’s formula was chosen to evaluate the mass flow rate through a channel [27]:

$$m = \mu \cdot k_a \cdot f \cdot \sqrt{\frac{\rho_1}{z} \cdot \frac{p_1^2 - p_2^2}{p_1}}, \quad (1)$$

where μ —nozzle’s flow ratio; k_a —adiabatic exponent; f —cross-sectional area, m^2 ; ρ_1 —inlet density, kg/m^3 ; p_1 —inlet pressure, Pa; p_2 —outlet pressure, Pa; z —the number of sequentially installed holes with sharp edges.

The coefficient μ , which considers the peculiarities of the abrasive material flow, was evaluated experimentally, as presented in Section 3.

2.2. Numerical Simulations

Numerical simulations were performed to establish the impact of the nozzle diameter on the actual and theoretical values of the mass flow rate. The studies were carried out using the FlowVision CFD 2.5.3 software (Idasugiyama-cho, Japan). The scheme of the numerical simulations is presented in Figure 1.

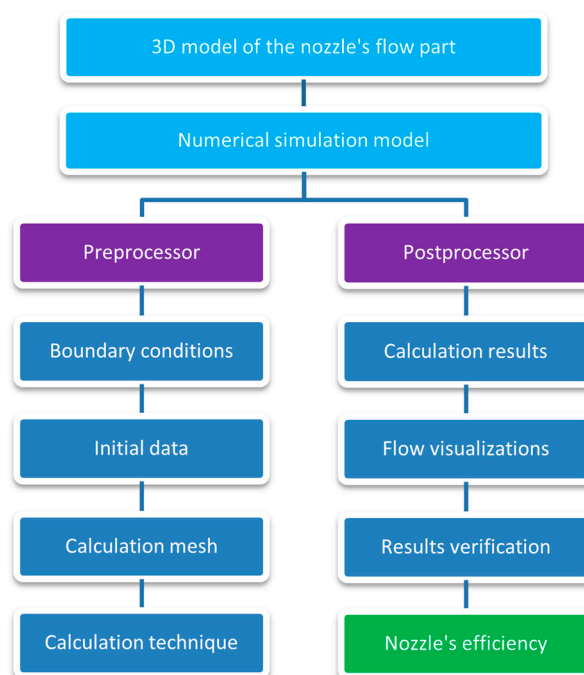


Figure 1. The scheme of the numerical simulations.

The flow model was fully compressible fluid with two-phase medium activation (particle option). This model allowed for simulating two-phase flows with particles. The carrier phase can be liquid or gas. Particles can be solid balls, drops, or bubbles. Abrasive particles have diameters from the 0.1–1.0 mm range.

An implicit calculation scheme was used. The particle motion model supplemented the compressible fluid model. Mutual influence of phases was assumed. Therefore, the carrier phase determines the particle trajectories. Particles, in turn, affect the flow through mass, momentum, and energy conservation laws.

The nozzle wall was impermeable and adiabatic, and the slip boundary condition was used for the continuous (gas) phase at the nozzle wall. The normal and tangent reflection coefficient 1.0 was applied for the dispersed (particle) phase.

At the inlet, the variable pressure was applied for the continuous phase. The dispersed phase had the same pressure and temperature as the continuous phase but with a variable mass fraction. Other boundary conditions were similar to the continuous phase.

The pressure drop to atmospheric was considered at the nozzle's outlet.

The temperature of particles was 300 K, the average particle size was 0.5 mm, the average distance between particles was 0.5 mm, and the particle surface degree was 1.0. Also, a coincidence of the particles' initial speed with the carrier phase's local speed was given.

A series of simulations using calculation mesh with different numbers of cells was carried out to identify the proper mesh selection. As a result, the calculation mesh was chosen with the number of cells of about 1.1×10^5 (Figure 2).

Figure 2 also contains the following geometric parameters: l —nozzle length, m ; h —wall thickness, m .

The program software operates with the following turbulence models: Spalart–Allmaras (S.A.), Menter's shear stress transport (SST), the low-Reynolds turbulent model (AKN) by Abe–Kondoh–Nagano, and the standard k - ϵ model. The previous research work [27] proved that the turbulence model does not significantly affect the change in pressure differences for channels with a high length-to-diameter ratio and, therefore, the mass flow rate through the gap. Moreover, throttling in a nozzle is similar to a labyrinth seal, where the pressure drop ratio p_1/p_2 does not exceed 1.2, and the walls of the calculated nozzle models are assumed to be hydraulically smooth.

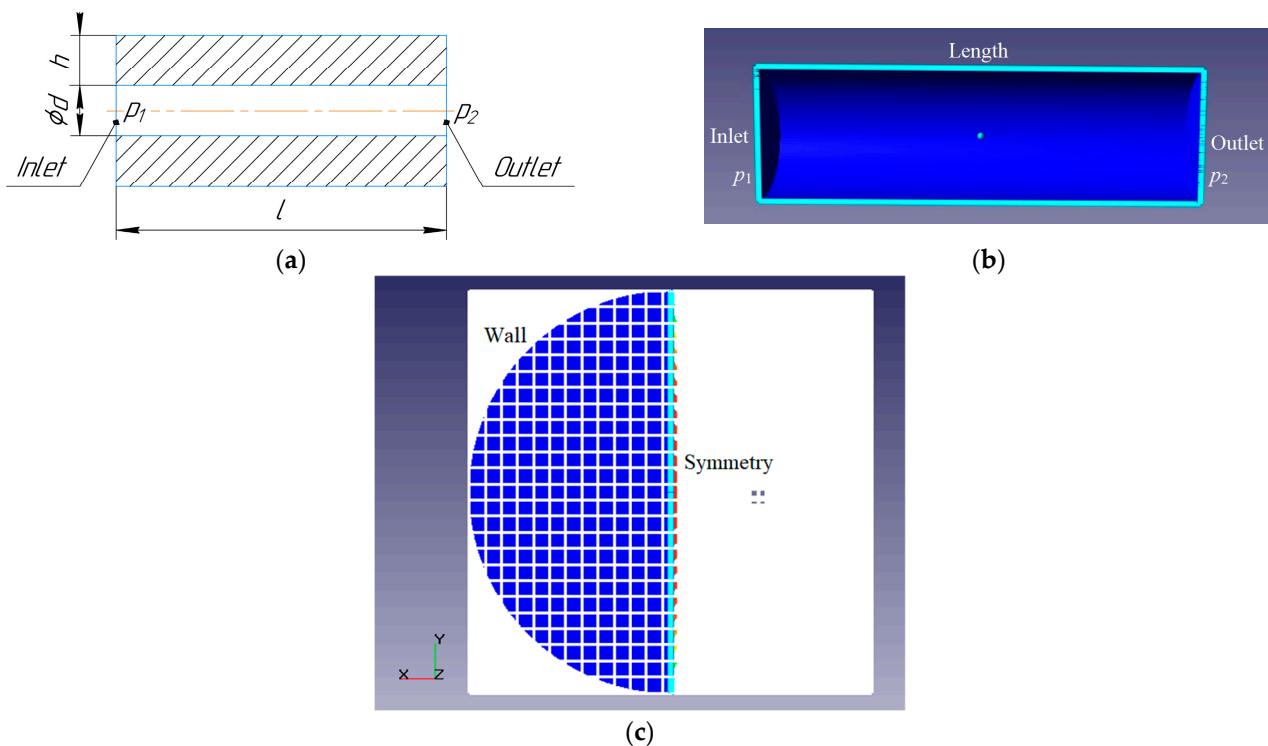


Figure 2. Drawing of the nozzle (a), its calculation area (b), and the calculation mesh (c).

Therefore, during the numerical simulations, the standard k - ε turbulence model was chosen because it agrees with most studies on gas flow. The corresponding equations for the turbulent kinetic energy k and the turbulent dissipation energy ε are as follows [28]:

$$\frac{\partial(\rho k)}{\partial t} + \frac{\partial(\rho k u_i)}{\partial x_i} = \frac{\partial}{\partial x_i} \left(\frac{\mu_t}{\sigma_k} \frac{\partial k}{\partial x_i} \right) + 2\mu_t E_{ij} E_{ij} - \rho \varepsilon; \quad (2)$$

$$\frac{\partial(\rho \varepsilon)}{\partial t} + \frac{\partial(\rho \varepsilon u_i)}{\partial x_i} = \frac{\partial}{\partial x_i} \left(\frac{\mu_t}{\sigma_\varepsilon} \frac{\partial \varepsilon}{\partial x_i} \right) + 2\mu_t E_{ij} E_{ij} C_{1\varepsilon} \frac{\varepsilon}{k} - \rho \frac{\varepsilon^2}{k} C_{2\varepsilon}, \quad (3)$$

where ρ —flow density, kg/m^3 ; t —time, s ; x_i —the i -th coordinate, m ; u_i —velocity component in the i -th direction, m/s ; μ_t —turbulent viscosity, $\text{Pa}\cdot\text{s}$; E_{ij} —the strain rate components ($i, j = 1, 2, 3$). Also, Equations (2) and (3) contain the following parameters: $\sigma_k = 1.0$, $\sigma_\varepsilon = 1.3$, $C_{1\varepsilon} = 1.44$, and $C_{2\varepsilon} = 1.92$ [29].

For the chosen model of a fully compressible fluid, the time step depends on the convergence of the pressure equations. As an example, the convergence of numerical simulation results by various physical parameters (pressure, velocity magnitude, and their pulsations) is presented in Figure 3.

Equality of mass flow rates at the inlet and the outlet was the primary convergence criterion for establishing the stationary flow mode in the compressor, which means the completion of the calculation.

The transition of the abrasive jet equipment to the operating mode was characterized by the pressure ratio of $p_1/p_2 = 1.98$.

2.3. Experimental Studies

Verification of numerical simulation results was carried out by conducting a series of experimental studies. The scheme of the experimental research is presented in Figure 4.

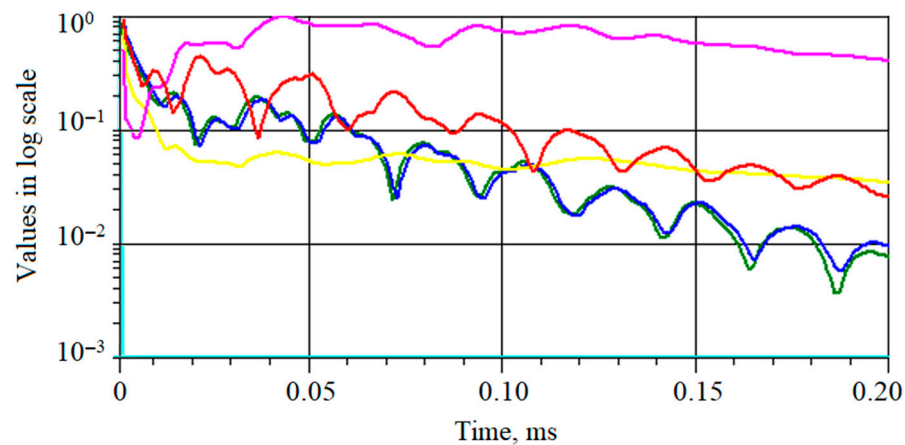


Figure 3. Convergence of the numerical simulation model by velocity (red line), pressure (green line), enthalpy (blue line), turbulent viscosity (yellow line), and concentration (magenta line).

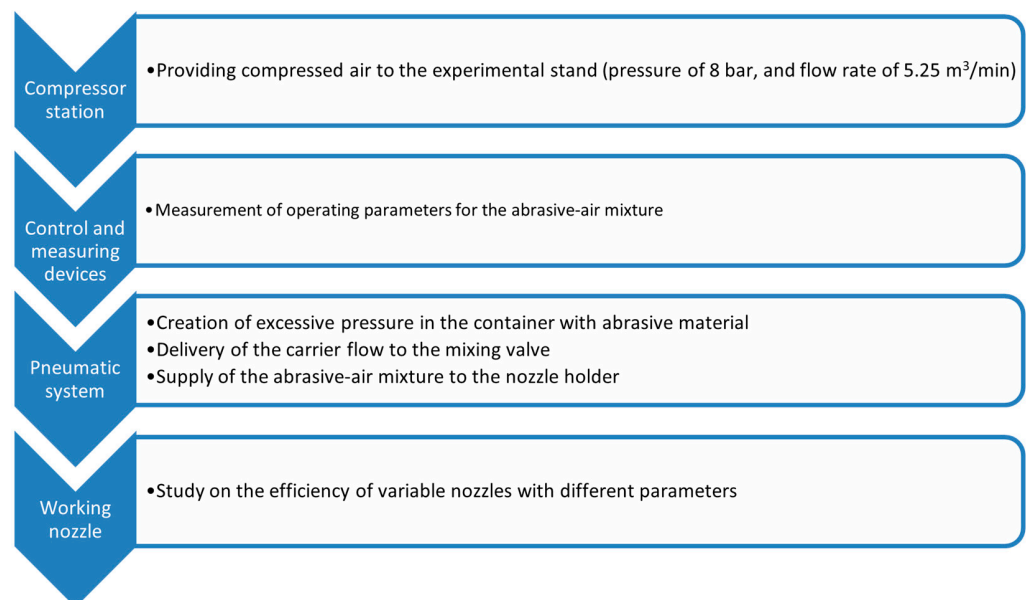


Figure 4. The scheme of the experimental research.

An experimental stand was installed to conduct the research (Figure 5).

The experimental stand includes the tested nozzle 6, a container with sand, a binding armature, and a portable compressor station with the following parameters: volume flow rate 5.25 m³/min, maximum injection pressure 800 kPa, and power of the electric motor 40 kW.

The compressor station can supply air to two abrasive jet devices at full capacity. However, due to a relatively energy-consuming compressor, frequent starts lead to overheating motor and the switching elements. Therefore, it is profitable to adjust the operation of the abrasive jet device in such a way as to reduce air consumption and the machining time per unit of the metal surface area.

The stand operates as follows. The abrasive material enters a hermetic container through sieve 2. Compressed air enters the tee 9 through the inlet valve 14, which picks up part of the abrasive material. Its supply is regulated by sand shutter 8. The air–abrasive mixture enters nozzle 6 through sleeve 10.

The experimental studies measured air flow rate, pressure, temperature, and amount of abrasive material. The volume of sand in the installation is 0.2 m³. River sand with a fraction in a range of 0.5–0.8 mm was used as an abrasive material.

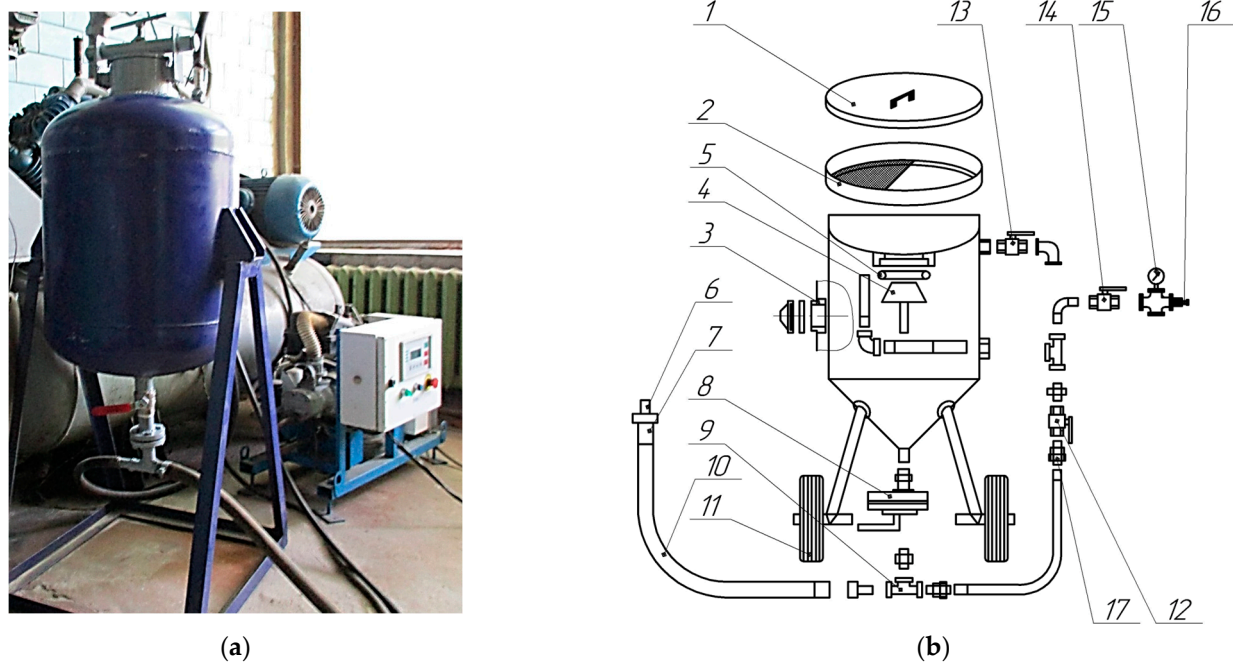


Figure 5. Experimental stand (a) and its design scheme (b): 1—cover; 2—sieve; 3—hatch; 4—closing cone; 5—closing ring; 6—abrasive jet ring; 7—nozzle holder; 8—sand shutter; 9—tee; 10—sleeve; 11—wheels; 12—air valve; 13—drain valve; 14—inlet valve; 15—manometer; 16—air connection; 17—quick connection.

The experimental setup allowed for research at variable operating pressure before and after the nozzle and changing the tested nozzles in a wide range of geometric parameters. The studied parameters were inlet pressure of 101 kPa, mass flow rate of 0.023–0.24 kg/s, nozzle diameter $d = 2\text{--}20$ mm, and length $l = 4\text{--}44$ mm. This allowed for rationally selecting the operating and geomantic parameters to improve the energy efficiency of the available working nozzles.

The values of the measurement errors for the actual flow rate of air and abrasive material were controlled before the gas flowmeter and directly in front of the nozzle. The “RG 250” flowmeter measured the air flow rate with an accuracy class of 1.0. The deformation manometer “D.M. 05-MP-3U” with a maximum pressure of 2 MPa and an accuracy class of 1.5 measured the pressure. The temperature was controlled by the “Testo 905-T2” thermometer. The amount of abrasive was measured by scales “KS10”, with a maximum loading of 10 kg and a tolerance of 1 g.

The measurement error of the main parameter μ was evaluated by indirect measurements technique [30].

3. Results

3.1. Experimental Results

The main geometric parameter of the nozzle is its inner diameter. Therefore, numerical experiments were conducted to establish its impact on the experimental and theoretical mass flow rate m , kg/s. As a result, the following power dependence of the mass flow rate on the nozzle diameter was proposed (Figure 6):

$$m(d) = m_{min} \cdot \left(\frac{d}{d_{min}} \right)^n, \quad (4)$$

where d —inner diameter of a nozzle, m; d_{min} —minimum nozzle’s diameter under consideration, m; m_{min} —mass flow rate for a nozzle with minimum diameter, kg/s; n —dimensionless regression coefficient.

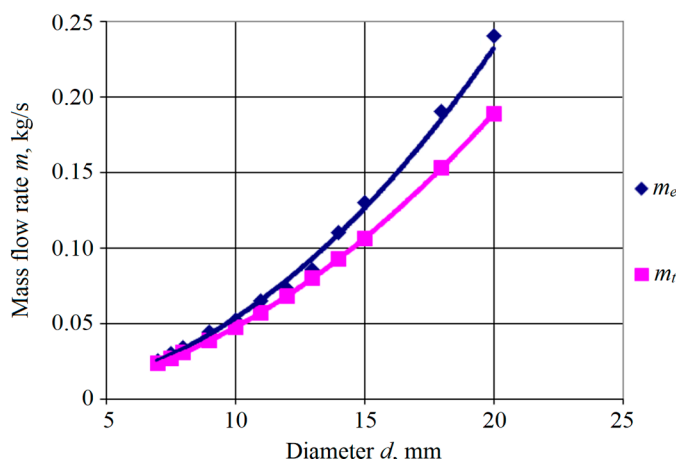


Figure 6. The dependencies of the mass flow rate on the diameter.

Figure 6 shows experimental m_e and theoretical m_t mass flow rates, respectively. Line 1 corresponds to the experimentally obtained mass flow rates m_e , kg/s. Line 2 is the theoretical curve for the mass flow rate m_t evaluated by Formula (1), kg/s.

The approximating dependence (4) reflects an increase in the mass flow rate m by an increase in the diameter d . Also, for the minimum diameter, the mass flow rate corresponds to its minimum value: $m(d_{min}) = m_{min}$.

Unknown parameters m_{min} and n were evaluated by the experimental data by minimizing the following mean square error (MSE) between logarithms of analytical dependence (4) and experimental data:

$$R_m(m_{min}, n) = \sum_{i=1}^N \left\{ \ln \left[m_{min} \cdot \left(\frac{d_i}{d_{min}} \right)^n \right] - \ln(m_i) \right\}^2 \rightarrow \min, \tag{5}$$

where i —experimental point index; N —the total number of experimental data; d_i — i -th nozzle’s diameter, m; m_i —experimentally obtained mass flow rate, kg/s.

MSE (5) reaches its minimum under the following conditions:

$$\frac{\partial R_m(m_{min}, n)}{\partial m_{min}} = \frac{\partial R_m(m_{min}, n)}{\partial n} = 0, \tag{6}$$

which directly corresponds to the following matrix equation:

$$\begin{bmatrix} N & \sum_{i=1}^N \ln\left(\frac{d_i}{d_{min}}\right) \\ \sum_{i=1}^N \ln\left(\frac{d_i}{d_{min}}\right) & \sum_{i=1}^N \ln^2\left(\frac{d_i}{d_{min}}\right) \end{bmatrix} \begin{Bmatrix} \ln(m_{min}) \\ n \end{Bmatrix} = \begin{Bmatrix} \sum_{i=1}^N \ln(m_i) \\ \sum_{i=1}^N \left[\ln(m_i) \ln\left(\frac{d_i}{d_{min}}\right) \right] \end{Bmatrix}. \tag{7}$$

The inverse matrix approach allowed for evaluating the estimated parameters:

$$m_{min} = \exp \left\{ \frac{\sum_{i=1}^N \ln(m_i) \cdot \sum_{i=1}^N \ln^2\left(\frac{d_i}{d_{min}}\right) - \sum_{i=1}^N \ln\left(\frac{d_i}{d_{min}}\right) \cdot \sum_{i=1}^N \left[\ln(m_i) \ln\left(\frac{d_i}{d_{min}}\right) \right]}{N \cdot \sum_{i=1}^N \ln^2\left(\frac{d_i}{d_{min}}\right) - \left[\sum_{i=1}^N \ln\left(\frac{d_i}{d_{min}}\right) \right]^2} \right\}; \tag{8}$$

$$n = \frac{N \cdot \sum_{i=1}^N \left[\ln(m_i) \cdot \ln\left(\frac{d_i}{d_{min}}\right) \right] - \sum_{i=1}^N \ln(m_i) \cdot \sum_{i=1}^N \ln\left(\frac{d_i}{d_{min}}\right)}{N \cdot \sum_{i=1}^N \ln^2\left(\frac{d_i}{d_{min}}\right) - \left[\sum_{i=1}^N \ln\left(\frac{d_i}{d_{min}}\right) \right]^2}. \tag{9}$$

According to Formulas (8) and (9), the evaluated parameters m_{min} and n were as follows: $m_{min} = 0.025$ kg/s; $n = 2.12$ for the case of m_e , and $n = 2.0$ —for the case of m_t .

Remarkably, the flow ratio also increases the mass flow rate. Therefore, to maintain the performance of a worn nozzle, 8–10 times more air and abrasive material consumption is required. This significantly increases the cost of AJM.

However, experimentally and theoretically obtained flow rates differed insignificantly. Therefore, the approximation of the flow ratio became linear. Particularly, Figure 7 demonstrates an increase in the flow rate by an increase in the inner diameter at a constant pressure drop:

$$\mu(d) = \mu_{min} + \alpha \cdot (d - d_{min}), \quad (10)$$

where μ_{min} —the flow ratio for a nozzle with minimum diameter d_{min} ; α —regression coefficient, m^{-1} .

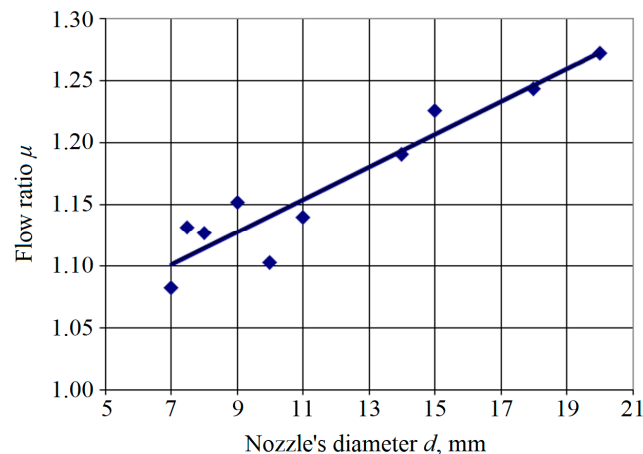


Figure 7. The dependence of the flow ratio on the diameter: dots—experimental data; line—approximating dependence (10).

The experimental data allowed for evaluating unknown parameters μ_{min} and α by minimizing the following MSE between logarithms of analytical dependence (10) and experimental data:

$$R_{\mu}(\mu_{min}, \alpha) = \sum_{i=1}^N (\mu_{min} + \alpha \cdot \Delta d_i - \mu_i)^2 \rightarrow \min, \quad (11)$$

where μ_i —experimentally obtained flow ratio; Δd_i —the difference between i -th nozzle's diameter and minimum diameter d_{min} , m.

$$\Delta d_i = d_i - d_{min}. \quad (12)$$

MSE (11) reaches its minimum under the following conditions:

$$\frac{\partial R_{\mu}(\mu_{min}, \alpha)}{\partial \mu_{min}} = \frac{\partial R_{\mu}(\mu_{min}, \alpha)}{\partial \alpha} = 0, \quad (13)$$

that directly correspond to the following matrix equation:

$$\begin{bmatrix} N & \sum_{i=1}^N \Delta d_i \\ \sum_{i=1}^N \Delta d_i & \sum_{i=1}^N \Delta d_i^2 \end{bmatrix} \begin{Bmatrix} \mu_{min} \\ \alpha \end{Bmatrix} = \begin{Bmatrix} \sum_{i=1}^N \mu_i \\ \sum_{i=1}^N (\mu_i \cdot \Delta d_i) \end{Bmatrix}. \quad (14)$$

The inverse matrix approach allowed for evaluating the estimated parameters:

$$\mu_{min} = \frac{\sum_{i=1}^N \mu_i \cdot \sum_{i=1}^N \Delta d_i^2 - \sum_{i=1}^N \Delta d_i \cdot \sum_{i=1}^N (\mu_i \cdot \Delta d_i)}{N \cdot \sum_{i=1}^N \Delta d_i^2 - \left(\sum_{i=1}^N \Delta d_i\right)^2}; \quad (15)$$

$$\alpha = \frac{N \cdot \sum_{i=1}^N (\mu_i \cdot \Delta d_i) - \sum_{i=1}^N \mu_i \cdot \sum_{i=1}^N \Delta d_i}{N \cdot \sum_{i=1}^N \Delta d_i^2 - \left(\sum_{i=1}^N \Delta d_i\right)^2}. \quad (16)$$

According to Formulas (15) and (16), the evaluated parameters μ_{min} and α were as follows: $\mu_{min} = 1.10$, and $\alpha = 1.27$.

The productivity of processing was also experimentally determined. It significantly depended on the pressure of compressed air. The flow rate depended on the nozzle diameter; it permanently increased due to wear.

Overall, the geometric and operational parameters of the nozzle are summarized in Table 1.

Table 1. The geometrical and operating parameters of the nozzle ¹.

d , mm	f , 10^{-5} mm ²	p_2 , kPa	m_e , kg/s	m_t , kg/s	μ
7.0	3.847	101	0.025	0.023	1.082
7.0	3.847	101	0.041	0.023	1.774
7.5	4.415	101	0.03	0.027	1.131
8.0	5.024	101	0.034	0.030	1.126
9.0	6.3585	101	0.044	0.038	1.152
10	7.850	101	0.052	0.047	1.103
11	9.499	101	0.065	0.057	1.139
12	11.304	101	0.073	0.068	1.075
13	13.267	101	0.085	0.080	1.066
14	15.386	101	0.110	0.092	1.190
15	17.663	101	0.130	0.106	1.225
18	25.434	101	0.190	0.153	1.243
20	31.400	101	0.240	0.189	1.272

¹ The unchangeable parameters are as follows: length $l = 22$ mm; inlet density $\rho_1 = 2.4$ kg/m³; inlet pressure $p_1 = 201$ kPa. The root mean square error does not exceed 5%.

The higher the ratio μ , the better the nozzle works. This is because the nozzle should pass the maximum amount of abrasive material, giving it maximum speed.

3.2. Numerical Simulation Results

Visualization of the distribution of gas-dynamic parameters in the nozzle provides essential information that predetermines a need for change in the flow organization by a change in its geometry.

As an example, the numerical simulation results of the flow in the nozzle are presented in Figures 8 and 9. These plots were built for different values of the nozzle diameter d and unchangeable values of the length ($l = 22$ mm) and pressure ratio $p_1/p_2 = 1.98$.

These visualizations show the distribution of abrasive flow parameters in the nozzle. Generally, they aim to understand flow organization and the effect of nozzle geometry on the flow. If vortices appear at certain operating parameters, it can be concluded how to influence the nozzle to improve its efficiency.

The difference in the flow structure of the working stream in nozzles with different values of the inner diameter draws attention. Particularly, for the case of $d = 7$ mm, non-uniformity of the flow parameters at the outlet from the nozzle was detected. However, this effect did not occur for higher diameters due to increased cross-sectional area. This effect did not also occur in the case of a single-phase flow.

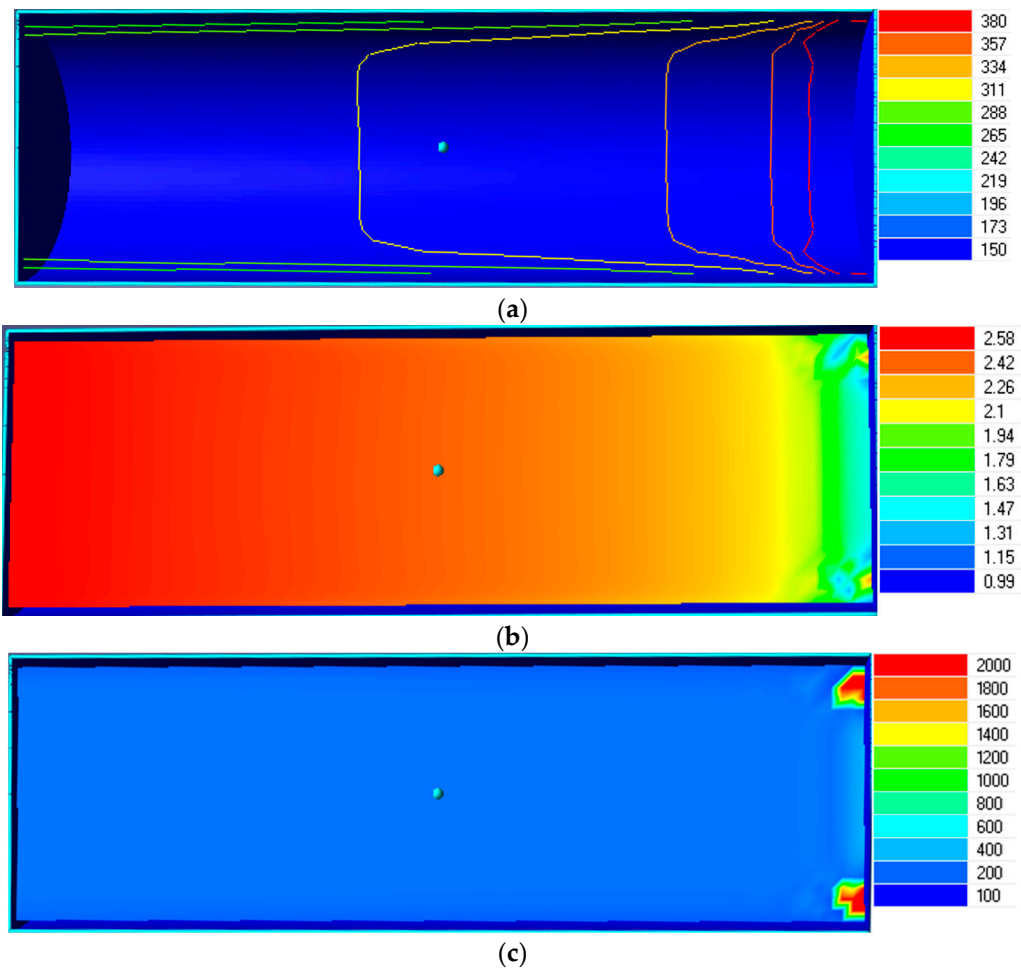


Figure 8. Visualization of the flow characteristics for the nozzle’s diameter $d = 7$ mm: (a) isolines of velocity magnitudes, m/s; (b) flow density, kg/m^3 ; (c) total pressure, kPa.

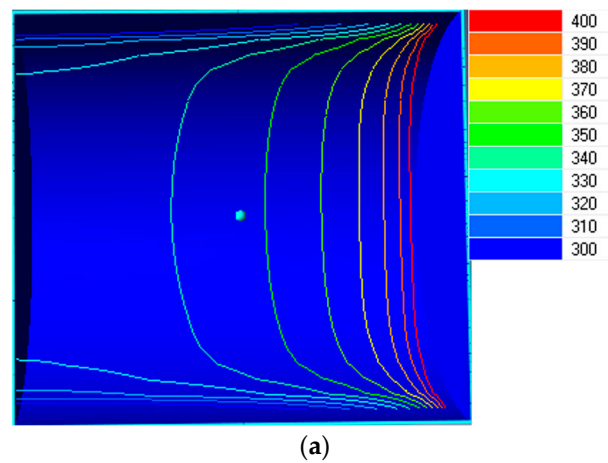


Figure 9. Cont.

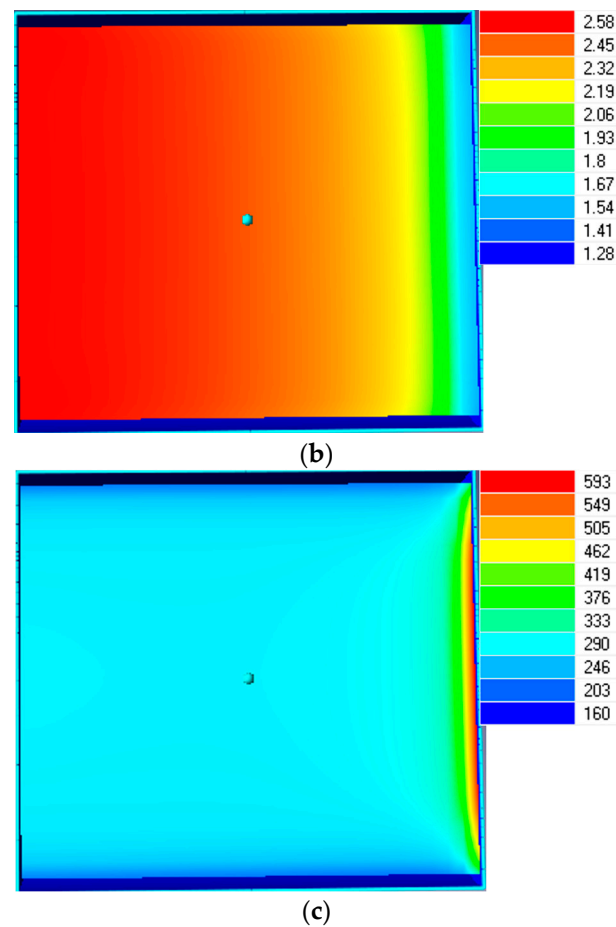


Figure 9. Visualization of the flow characteristics for the nozzle's diameter $d = 20$ mm: (a) isolines of velocity magnitudes, m/s; (b) flow density, kg/m³; (c) total pressure, kPa.

Moreover, before the outlet cross-section of the nozzle, a blocking of part of the flow was detected. This was due to localized centers of increasing operating parameters. This effect also disappeared as the diameter increased.

The numerical simulation results were compared with the experimental results. The discrepancy was within 5%.

3.3. Choice of the Rational Geometry

After considering the peculiarities of the air–abrasive mixture flow in nozzles of various geometric parameters, additional studies were carried out to evaluate the rational design of the nozzle (Table 2).

Table 2. The geometrical and operational parameters of the studied nozzles.

No.	d , mm	l , mm	m_e , kg/s	m_t , kg/s	μ
1	2	22	0.002	0.002	0.981
2	4	22	0.008	0.008	1.060
3	5	22	0.013	0.012	1.060
4	6	22	0.019	0.017	1.119
5	7	4	0.044	0.023	1.904
6	7	44	0.024	0.023	1.038
7	7	44	0.053	0.023	2.272
8	14	44	0.100	0.092	1.082

Table 2 demonstrates an increase in the flow ratio μ with an increase in the nozzle diameter d . This is because the mass flow rate of the abrasive mixture through the nozzle increases according to the continuity equation.

The average value of the ratio μ is about 1.0. However, variant 7 is the most rational. It has the highest value of the flow ratio of about 2.3. Nevertheless, in variant 5, a significant decrease in the nozzle length l up to 4 mm led to a significant increase in mass flow rate m of about 1.9 kg/s. This leads to increasing the mass flow rate of the mixture.

Overall, due to the rational choice of the geometric parameters of the abrasive jet device, the specific machining time decreased from 540 s to 120 s per unit of metal surface area. The energy efficiency of the corresponding compressor equipment also increased by 84%. The energy-efficient nozzle designs also confirmed their effectiveness on the experimental stand.

4. Discussion

From the analysis of the available types of nozzles for AJM, it can be concluded that the primary trend in the improvement of nozzles is the use of super-hard and wear-resistant materials (e.g., boron carbide [31,32], silicon carbide [33], and tungsten carbide [34]). These materials improve the performance characteristics of the nozzle and, accordingly, extend their durability. However, the new materials mentioned above are highly expensive. Moreover, there is loss in the energy efficiency of the corresponding compressor equipment during AJM.

Therefore, the rational choice of nozzle geometry was proposed to decrease the costs of nozzle design from available materials and increase the energy efficiency of the abrasive jet equipment. This reduced the hydraulic losses from the friction of the abrasive material with the walls.

The numerical simulation results for a two-phase flow through a nozzle agree with the research work by Van den Berghe [9]. Particularly, Figure 6 shows an increase in the mass flow rate with an increase in its diameter. This effect also corresponds to the research work by Sychuk et al. [24].

The nature of the obtained approximation curves presented in Figure 7 is explained by a disproportionate change in the operating characteristics of the nozzle to a change in its diameter. This fact also agrees with the research work by Xu et al. [10]. The results can also be justified by [15] because the rational choice of geometrical parameters significantly influences energy efficiency.

Moreover, the dependencies in Figure 7 demonstrate the tendency to increase the flow ratio of the air–abrasive mixture in the nozzle and its mass flow rate with an increase in its internal diameter at constant pressure drop values. This result also corresponds to the research works by Li Aronson et al. [11,12].

The obtained results also allow for further improving the operating processes in jet apparatuses [35] and modeling vortex chambers [36].

5. Conclusions

The article presents the results of numerical and experimental studies of nozzles for AJM for variable geometric parameters. The research was carried out to find reserves in increasing the nozzle performance and ensuring the energy efficiency of abrasive jet equipment.

As a result, the difference in the working flow structure in nozzles with different inner diameters in a range of 7–20 mm was established. Particularly for the diameter of 7 mm, non-uniform flow parameters occurred at the outlet. Also, it was established that reducing the nozzle's length to 4 mm significantly increases the mass flow rate.

The experimental studies and analytical approximations allowed for evaluating conditions to increase the energy efficiency of the abrasive jet equipment. Particularly, the machining time per unit of metal surface area was reduced by 4.5 times. Since the flow ratio predetermines the main parameters of the working nozzle and, consequently, the

abrasive jet device, it was chosen as an efficiency indicator. Overall, the energy efficiency of compressor equipment for AJM was increased by 84%.

Thus, increasing the efficiency of the abrasive jet nozzle was realized by reducing the contact area of the working two-phase flow. Due to this, the friction of the abrasive material with the walls was reduced. As a result, AJM was accelerated, and the energy consumption of the corresponding compressor equipment was reduced. This made the nozzle more effective.

Further research directions will be aimed at improving the energy efficiency of AJM with porous nozzles.

Author Contributions: Conceptualization, V.B. and I.P.; methodology, V.B.; software, J.M.; validation, I.P. and J.M.; formal analysis, V.B. and J.M.; investigation, V.B., I.P. and J.M.; resources, J.M.; data curation, I.P. and J.M.; writing—original draft preparation, V.B. and I.P.; writing—review and editing, J.M.; visualization, V.B. and J.M.; supervision, I.P.; project administration, I.P.; funding acquisition, I.P. and J.M. All authors have read and agreed to the published version of the manuscript.

Funding: The research was funded by Ulam NAWA Programme, ordered by the Polish National Agency for Academic Exchange, grant number BPN/ULM/2022/1/00042.

Data Availability Statement: The data are available from the corresponding author on request.

Acknowledgments: The authors appreciate the additional support of the project VEGA 1/0704/22 granted by the Ministry of Education, Science, Research and Sport of the Slovak Republic.

Conflicts of Interest: The authors declare no conflict of interest.

Abbreviations

AJM	Abrasive jet machining	
CFD	Computational fluid dynamics	
d	Nozzle's inner diameter	m
d_i	i -th nozzle's diameter	m
d_{min}	Minimum nozzle's diameter	m
Δd_i	Difference of diameters	m
f	Cross-sectional area	m ²
i, j	Indexes	
k	Turbulent kinetic energy	m ² /s ²
k_a	Adiabatic exponent	
l	Nozzle length	m
m	Mass flow rate	kg/s
m_e	Experimental mass flow rate	kg/s
m_i	Experimentally obtained mass flow rate	kg/s
m_{min}	Minimum mass flow rate	kg/s
m_t	Theoretical mass flow rate	kg/s
MSE	Mean square error	
n	Dimensionless regression coefficient	
N	Total number of experimental data	
R_m	Mean square error	
t	Time	s
u_i	Velocity component in i -th direction	m/s
x_i	i -th coordinate	m
z	Number of sequentially installed holes	
α	Regression coefficient	m ⁻¹
μ	Nozzle's flow ratio	
μ_i	Experimentally obtained flow ratio	
μ_{min}	Minimum flow ratio	

ε	Turbulent dissipation energy	m^2/s^2
ρ	Flow density	kg/m^3
ρ_1	Inlet density	kg/m^3
p_1	Inlet pressure	Pa
p_2	Outlet pressure	Pa
μ_t	Turbulent viscosity	Pa·s
E_{ij}	Strain rate	

References

- Fesenko, A.; Basova, Y.; Ivanov, V.; Ivanova, M.; Yevsiukova, F.; Gasanov, M. Increasing of equipment efficiency by intensification of technological processes. *Period. Polytech. Mech. Eng.* **2019**, *63*, 67–73. [\[CrossRef\]](#)
- Arana-Landín, G.; Uriarte-Gallastegi, N.; Landeta-Manzano, B.; Laskurain-Iturbe, I. The contribution of lean Management—Industry 4.0 technologies to improving energy efficiency. *Energies* **2023**, *16*, 2124. [\[CrossRef\]](#)
- Kotliar, A.; Basova, Y.; Ivanov, V.; Murzabulatova, O.; Vasylytova, S.; Litvynenko, M.; Zinchenko, O. Ensuring the economic efficiency of enterprises by multi-criteria selection of the optimal manufacturing process. *Manag. Prod. Eng. Rev.* **2020**, *11*, 52–61. [\[CrossRef\]](#)
- Rudawska, A.; Danczak, I.; Müller, M.; Valasek, P. The effect of sandblasting on surface properties for adhesion. *Int. J. Adhes. Adhes.* **2016**, *70*, 176–190. [\[CrossRef\]](#)
- Peñuela-Cruz, C.E.; Márquez-Herrera, A.; Aguilera-Gómez, E.; Saldaña-Robles, A.; Mis-Fernández, R.; Peña, J.L.; Caballero-Briones, F.; Loeza-Poot, M.; Hernández-Rodríguez, E. The effects of sandblasting on the surface properties of magnesium sheets: A statistical study. *J. Mater. Res. Technol.* **2023**, *23*, 1321–1331. [\[CrossRef\]](#)
- Pruszczńska, E.; Pietnicki, K.; Klimek, L. Effect of the abrasive blasting treatment on the quality of the pressed ceramics joint for a metal foundation. *Arch. Mater. Sci. Eng.* **2016**, *78*, 17–22. [\[CrossRef\]](#)
- Ahmed, F.; Chen, W. Investigation of steam ejector parameters under three optimization algorithm using ANN. *Appl. Therm. Eng.* **2023**, *225*, 120205. [\[CrossRef\]](#)
- Van den Berghe, J.; Dias, B.R.B.; Bartosiewicz, Y.; Mendez, M.A. A 1D model for the unsteady gas dynamics of ejectors. *Energy* **2023**, *267*, 126551. [\[CrossRef\]](#)
- Yan, J.; Li, Z.; Zhang, H. Investigation on key geometries optimization and effect of variable operating conditions of a transcritical R744 two-phase ejector. *Appl. Therm. Eng.* **2023**, *230*, 120733. [\[CrossRef\]](#)
- Xu, Y.; Li, Q.; Li, B.; Guan, Z. Numerical simulation study of hydraulic fracturing nozzle erosion in deep well. *Front. Phys.* **2022**, *10*, 947094. [\[CrossRef\]](#)
- Li, A.; Chen, J.; Xi, G.; Huang, Z. Numerical investigation of the effect of primary nozzle geometries on flow structure and ejector performance for optimal design. *J. Mech. Sci. Technol.* **2023**, *37*, 2139–2148. [\[CrossRef\]](#)
- Aronson, K.E.; Ryabchikov, A.Y.; Zhelonkin, N.V.; Brezgin, D.V.; Demidov, A.L.; Balakin, D.Y. Features of the development and operation of multistage steam jet ejectors. *Therm. Eng.* **2023**, *70*, 245–253. [\[CrossRef\]](#)
- Bañon, F.; Sambruno, A.; Batista, M.; Simonet, B.; Salguero, J. Surface quality and free energy evaluation of S275 steel by shot blasting, abrasive water jet texturing and laser surface texturing. *Metals* **2020**, *10*, 290. [\[CrossRef\]](#)
- Kwon, D.-K.; Lee, J.-H. Performance improvement of micro-abrasive jet blasting process for al 6061. *Processes* **2022**, *10*, 2247. [\[CrossRef\]](#)
- Sychuk, V.; Zabolotnyi, O.; McMillan, A. Developing new design and investigating porous nozzles for abrasive jet machine. *Powder Metall. Met. Ceram.* **2015**, *53*, 600–605. [\[CrossRef\]](#)
- Hao, X.; Yan, J.; Gao, N.; Volovyk, O.; Zhou, Y.; Chen, G. Experimental investigation of an improved ejector with optimal flow profile. *Case Stud. Therm. Eng.* **2023**, *47*, 103089. [\[CrossRef\]](#)
- Kartal, V.; Emiroglu, M.E. Effect of nozzle type on local scour in water jets: An experimental study. *Ocean Eng.* **2023**, *277*, 114323. [\[CrossRef\]](#)
- Xi, X.; Xin, Y.; Duan, D.; Zhang, B. Experimental investigation on the performance of a novel resonance-assisted ejector under low pressurization. *Energy Convers. Manag.* **2023**, *280*, 116778. [\[CrossRef\]](#)
- Han, X.; Xiao, J.; Yu, F.; Zhao, W. Relationships and mechanisms of sand grain promotion on nozzle cavitation flow evolution: A numerical simulation investigation. *J. Therm. Sci.* **2022**, *31*, 2385–2410. [\[CrossRef\]](#)
- Fesenko, A.; Yevsiukova, F.; Basova, Y.; Ivanova, M.; Ivanov, V. Prospects of using hydrodynamic cavitation for enhancement of efficiency of fluid working medium preparation technologies. *Period. Polytech. Mech. Eng.* **2018**, *62*, 269–276. [\[CrossRef\]](#)
- Zabolotnyi, O.; Povstyanoy, O.; Somov, D.; Sychuk, V.; Svirzhevskiy, K. Technology of Obtaining Long-Length Powder Permeable Materials with Uniform Density Distributions. In *World Congress on Engineering and Technology; Innovation and Its Sustainability 2018. WCETIS 2018*; Beltran, A., Jr., Lontoc, Z., Conde, B., Serfa Juan, R., Dizon, J., Eds.; EAI/Springer Innovations in Communication and Computing; Springer: Cham, Switzerland, 2022; pp. 63–78. [\[CrossRef\]](#)
- Zabolotnyi, O.; Sychuk, V.; Somov, D. Obtaining of Porous Powder Materials by Radial Pressing Method. In *Advances in Design, Simulation and Manufacturing. DSMIE 2018*; Ivanov, V., Trojanowska, J., Pavlenko, I., Zajac, J., Peraković, D., Eds.; Lecture Notes in Mechanical Engineering; Springer: Cham, Switzerland, 2019; pp. 186–198. [\[CrossRef\]](#)

23. Somov, D.; Zabolotnyi, O.; Polinkevich, R.; Valetskyi, B.; Sychuk, V. Experimental Vibrating Complex for the Research of Pressing Processes of Powder Materials. In *Advances in Design, Simulation and Manufacturing II. DSMIE 2019*; Martsynkovskyy, V., Tarelnyk, V., Konoplianchenko, I., Gaponova, O., Dumanchuk, M., Eds.; Lecture Notes in Mechanical Engineering; Springer: Cham, Switzerland, 2020; pp. 321–329. [[CrossRef](#)]
24. Sychuk, V.; Zabolotnyi, O.; Somov, D. Technology of Effective Abrasive Jet Machining of Parts Surfaces. In *Advances in Design, Simulation and Manufacturing. DSMIE 2018*; Ivanov, V., Trojanowska, J., Pavlenko, I., Zajac, J., Peraković, D., Eds.; Lecture Notes in Mechanical Engineering; Springer: Cham, Switzerland, 2019; pp. 166–176. [[CrossRef](#)]
25. Povstyanoi, O.Y.; Sychuk, V.A.; McMillan, A.; Rud', V.D.; Zabolotnyi, O.V. Metallographic analysis and microstructural image processing of sandblasting nozzles produced by powder metallurgy methods. *Powder Metall. Met. Ceram.* **2015**, *54*, 234–240. [[CrossRef](#)]
26. Bondarenko, G.; Vanyeyev, S.; Baga, V.; Rodymchenko, T.; Bashlak, I. Increase of Efficiency of Turbine Setting Based on Study of Internal Flows. In *Advances in Design, Simulation and Manufacturing. DSMIE 2018*; Ivanov, V., Trojanowska, J., Pavlenko, I., Zajac, J., Peraković, D., Eds.; Lecture Notes in Mechanical Engineering; Springer: Cham, Switzerland, 2019; pp. 237–246. [[CrossRef](#)]
27. Baha, V. Improvement of Calculation and Design Methods of Pneumatic Shaft Seals Based on Workflow Simulation. Ph.D. Thesis, Sumy State University, Sumy, Ukraine, 1 July 2015. Available online: https://essuir.sumdu.edu.ua/bitstream/123456789/40851/6/diss_baha.pdf (accessed on 16 August 2023).
28. Bradshaw, P. Turbulent secondary flows. *Annu. Rev. Fluid Mech.* **1987**, *19*, 53–74. [[CrossRef](#)]
29. Versteeg, H.K.; Malalasekera, W. *An Introduction to Computational Fluid Dynamics: The Finite Volume Method*; Pearson Education: London, UK, 2007.
30. Kosheleva, O.; Kreinovich, V. Error estimation for indirect measurements: Interval computation problem is (slightly) harder than a similar probabilistic computational problem. *Reliab. Comput.* **1999**, *5*, 81–95. [[CrossRef](#)]
31. Jianxin, D. Erosion wear of boron carbide ceramic nozzles by abrasive air-jets. *Mater. Sci. Eng. A* **2005**, *408*, 227–233. [[CrossRef](#)]
32. Jianxin, D.; Sun, J. Sand erosion performance of B₄C based ceramic nozzles. *Int. J. Refract. Met. Hard Mater.* **2008**, *26*, 128–134. [[CrossRef](#)]
33. Karadimas, G.; Salonitis, K. Ceramic matrix composites for aero engine applications—A review. *Appl. Sci.* **2023**, *13*, 3017. [[CrossRef](#)]
34. Pătirnac, I.; Ripeanu, R.G.; Laudacescu, E. Abrasive flow modelling through active parts water jet machine using CFD simulation. *IOP Conf. Ser. Mater. Sci. Eng.* **2019**, *724*, 012001. [[CrossRef](#)]
35. Merzliakov, I.; Pavlenko, I.; Chekh, O.; Sharapov, S.; Ivanov, V. Mathematical modeling of operating process and technological features for designing the vortex type liquid-vapor jet apparatus. In *Advances in Design, Simulation and Manufacturing II. DSMIE 2019*; Martsynkovskyy, V., Tarelnyk, V., Konoplianchenko, I., Gaponova, O., Dumanchuk, M., Eds.; Lecture Notes in Mechanical Engineering; Springer: Cham, Switzerland, 2020; pp. 613–622. [[CrossRef](#)]
36. Merzliakov, I.; Pavlenko, I.; Ochowiak, M.; Ivanov, V.; Agarwal, P. Flow modeling in a vortex chamber of a liquid–steam jet apparatus. *Processes* **2022**, *10*, 984. [[CrossRef](#)]

Disclaimer/Publisher's Note: The statements, opinions and data contained in all publications are solely those of the individual author(s) and contributor(s) and not of MDPI and/or the editor(s). MDPI and/or the editor(s) disclaim responsibility for any injury to people or property resulting from any ideas, methods, instructions or products referred to in the content.